Lighting Up at High Potential: Effects of Voltage and Emitter Size in Nanoelectrospray Ionization

Jacob S. Jordan, Zachary M. Miller, Conner C. Harper, Emeline Hanozin and Evan R. Williams*

Department of Chemistry, University of California, Berkeley, California, 94720-1460

*To whom correspondence should be addressed

e-mail: erw@berkeley.edu

Abstract

Effects of electrospray emitter voltage on cluster size and abundance formed from aqueous CsI were investigated with emitter tip diameters between 260 ± 7 nm and 2.45 ± 0.30 μm. Cluster size increases with increasing voltage, increasing solution concentration and increasing emitter diameter consistent with formation of larger initial droplet sizes. For emitters with tip diameters above ~1 μm, varying the voltage either up or down leads to reproducible extents of cluster formation. In contrast, higher voltages with submicron diameter emitters can lead to only Cs^+ and $Cs(H_2O)^+$ and no clusters. This change in ion formation reproducibly occurs at spray potentials >1.3 kV for 260 nm emitters and appears to be induced by a corona discharge and material build-up at the emitter tip. Under conditions where abundant Cs^+ is observed and no clusters are formed, ions such as K^+ and Cu^{1+} are also observed but ions with more negative solvation energies, such as Ba^{2+}, are not. Similarly, ions from bradykinin and ubiquitin are observed pre-discharge but not post discharge. Ions with more positive solvation energies can desorb directly from the air-water interface that is created at the tip of these emitters whereas ions with more negative solvation energies as well as peptide and protein ions do not. These results indicate that ion desorption directly from solution can occur and similar experiments with even smaller emitters may lead to new insights into ion formation in electrospray ionization.

Introduction

The nanoflow regime of electrospray ionization (<1 μL min^{-1} flow rates) can lead to higher ionization efficiency and lower sample consumption than conventional electrospray ionization that uses large bore capillaries.[1,2] Nanospray also enables more reproducible ion formation from solvents that have high surface tension, most notably aqueous solutions that contain volatile buffers.[1,2] These advantages make nanospray an indispensable technique in native mass spectrometry. Nanospray emitters that have tips with inner diameters <1 μm have some additional advantages, including the ability to obtain charge-state resolved spectra of proteins and other molecules in standard biochemical buffers, such as Tris or 1x phosphate buffered saline solutions, that contain high concentrations of nonvolatile salts (e.g., ≥150 mM NaCl).[3–6] The initial droplet size formed by submicron emitters is less than 100 nm.[4,7–9] At an initial droplet diameter of 100 nm, there will be, on average, only one analyte molecule per droplet at concentrations below 3 μM.[10] At even lower concentrations or droplet diameters, the majority of nanodrops will not contain an analyte molecule. Under these conditions, nonvolatile salts are separated from analytes because most of the salts partition into nanodrops that do not contain an analyte ion. Nonspecific aggregation of analytes within the ESI droplet can also be reduced or prevented using sufficiently small diameter emitters. Narrow bore emitters have been used to investigate small molecule clusters,[10,11] as well as ligand-protein,[12–18] ligand-DNA,[19,20] and protein-protein[21] complexes without interference from nonspecific aggregation during the ESI process.

The diameters and size distribution of droplets that are initially formed in electrospray depends on many factors, including solution composition and surface tension,[22,23] viscosity,[24,25] conductivity,[23,26,27] sheath gas flow,[28,29] electrospray voltage,[22,23,26,30,31] capillary diameter,[23] distance from the capillary to the instrument inlet,[23] spray mode,[23,32] and solution flow rate.[22]

Droplets produced during ESI from larger diameter capillaries (>20 μm) can be characterized using optical methods, including phase doppler anemometry/interferometry, flash shadowgraphy, or microscope imaging and are typically on the 1 – 100 μm size scale across a range of solution and electrospray conditions.[23] Lower solution flow rates[22,33–36] and lower electrospray voltages[26,30,37] have been correlated with the production of smaller initial droplet sizes, although some deviations from this trend have been noted due to changes in the spray mode at different spray potentials.[37]

The initial nanodrops that are produced by nanoelectrospray ionization (nESI) emitters with tip diameters of a few microns or less are too small to size using standard optical methods, but some information about size and size distributions has been obtained from more indirect methods. Davidson *et al.* combined charge reduction with differential mobility analysis to determine the size of sucrose clusters formed from an aqueous sucrose solution with emitters that had 1 – 3 μm diameter tips.[7] From these results, they concluded that the initial droplet size was ~60 nm, or ~1/17th the emitter tip diameter. The average droplet diameter increased to ~500 nm with an increase in spray voltage from 0.8 kV to 1.5 kV. The initial size of droplets from nanospray emitters with small diameter tips was also estimated based on trends in sodium adduction to a protein as a function of emitter tip size. Sodium adduction to protein ions significantly decreases when there is less than one protein molecule per droplet, from which an estimate of the initial ESI droplet diameters of ~1/14th – 1/20th the emitter tip diameter was reported.[4] Calculations from Li *et al.* based on the measured flow rate and ionization current from submicron tips also resulted in droplet diameters that were 1/6th – 1/32nd the emitter diameter.[9] This relationship between tip diameter and droplet diameter also appears to be true for solvents other than water. Cooks and coworkers formed droplets containing rhodamine B onto a

glass coverslip and used fluorescence microscopy to investigate the droplet sizes produced from a solution of 9:1 methanol:glycerol with ~5 μm, ~10 μm, and ~20 μm diameter emitters.[8] The droplet size distribution from ~5 μm emitters at 1.5 kV spray voltage was broad with a center at 335 nm, or ~1/15th the emitter diameter, and the droplet diameter increased with increasing spray voltage to 463 nm at 2.5 kV. Droplets produced from ~10 μm and ~20 μm diameter emitters were larger than those produced from ~5 μm emitters.[8] These and other results indicate that there is a clear trend toward smaller initial droplet sizes with decreasing emitter tip sizes and larger initial droplet sizes with increasing spray voltage.

Here, effects of both voltage and emitter tip diameter are investigated for emitters with inner diameters between 260 ± 7 nm and 2.45 ± 0.30 μm. Emitters with diameters above ~1 μm show expected trends in ion formation as a function of emitter tip size and voltage whereas emitters with tip diameters below ~1 μm show unusual behavior when the electrospray voltage exceeds a threshold value that is commonly used with the larger emitters. Corona discharge and a change in ion formation mechanism after discharge provides insights into different ways that ions can be formed with electrostatic potentials.

Materials and Methods

Borosilicate nanoelectrospray emitters (1.0 mm outer diameter, 0.78 mm inner diameter, with filament, Part #BF100-78-10, Sutter Instrument, Novato, CA) were pulled to final inner diameters of 260 ± 7 nm, 608 ± 17 nm, 1.75 ± 0.11 μm, and 2.45 ± 0.30 μm using a Sutter Instrument Flaming/Brown P-87 pipette puller.[38] Emitters were imaged without sputter coating using a Hitachi TM-1000 scanning electron microscope (Tokyo, Japan) at the Electron Microscopy Laboratory at the University of California, Berkeley.

All mass spectral data were acquired using a Waters Q-TOF Premier mass spectrometer (Milford, MA). The pressure of argon in the collision cell was ~4 mbar and the sample cone, extraction cone, and ion guide voltages were 20.0 V, 2.0 V, and 2.0 V, respectively. A microscope consisting of a Dino-Lite digital camera and an objective lens (Olympus CK20, Tokyo, Japan) was mounted to the source region of the mass spectrometer to monitor emitter tips during electrospray. Emitters were positioned ~3 mm from the instrument inlet and a voltage between 0.4 kV and 1.5 kV was applied to a platinum wire that was in contact with an aqueous solution of 10 mM or 100 μM CsI (Sigma-Aldrich, St. Louis, MO). The voltage was increased or decreased in increments of 100 V every 15 s and the cluster distribution was measured as a function of spray voltage. All data were analyzed using MassLynx v. 4.1.

The emitter flow rate was determined by measuring the mass of the emitter loaded with ~10 μL of solution using an Ohaus Analytical Plus balance (Parsippany, NJ) before and after electrospray at a voltage of 1.0 kV for 5 minutes.[39] To measure the solution flow rate after corona discharge, the spray voltage was increased to ~1.5 kV until corona discharge was observed and then reduced back to 1.0 kV for 5 minutes followed by a mass measurement. To measure mass loss due to evaporation, the mass of the emitter and solution was measured before and after 5 minutes in the source with no spray voltage applied. The same emitter was used for measuring the mass loss due to evaporation, during electrospray, and after corona discharge to reduce variability caused by tip-to-tip differences in size and shape. Reported flow rates are the average of three replicate experiments.

Solutions of 10 mM tetraethylammonium chloride (TEACl), RbCl, KCl, NaCl, LiCl, CuCl (saturated solution), and $BaCl_2$ were mixed 1:1 with 10 mM CsCl (final concentration of 5 mM each) in MilliQ water. Bradykinin and ubiquitin solutions were prepared in 1:1 $BaCl_2$:CsCl

(5 mM each) to a final peptide or protein concentration of 10 μM. All reagents were obtained from Sigma-Aldrich and were used without further purification.

Results and Discussion

Effects of Emitter Tip Size and Voltage on CsI Cluster Distributions

The effects of nanoelectrospray emitter tip size and electrospray voltage on the formation of CsI clusters formed from either 100 μM or 10 mM aqueous solutions was investigated with emitters that have tip diameters between 260 ± 7 nm and 2.45 ± 0.30 μm and with electrospray voltages between 0.4 kV and 1.5 kV. At a given emitter tip diameter and solution concentration, higher spray voltage results in greater abundances of $[Cs_nI_{n-x}]^{x+}$ (x = 1, 2, 3). This effect is illustrated for singly charged clusters formed from a 10 mM aqueous CsI solution using an emitter with a 2.45 μm diameter tip (Figure 1a). Cs^+ and cluster ion abundances were normalized to the total mass of Cs by weighting each cluster abundance by the number of Cs atoms in the cluster (e.g., Cs_2Cl abundance multiplied by two, Cs_3Cl_2 abundance multiplied by three). The abundance of the Cs^+ ion decreases from 8.4 ± 2.3% of the Cs mass at 0.7 kV to 3.4 ± 0.4% at 1.5 kV. The fraction of singly charged clusters relative to multiply charged clusters decreases from 74.0 ± 2.0% to 59.1 ± 1.7% of the total Cs mass at these respective spray voltages reflecting the shift in the population to larger clusters (Figure 1a) that are more highly charged. The cluster abundances shift to smaller size as voltage is reduced from the maximum of 1.5 kV (Figure 1a) and the results at each voltage are highly reproducible. The difference between the abundance of Cs^+ at 1.0 kV on the increasing and decreasing voltage ramp is only ~0.1%. A similar trend occurs for emitters with diameters of 1.75 μm, 608 nm, and 260 nm (Figure 1b, 1c, 1d, respectively) when the initially low voltage is increased.

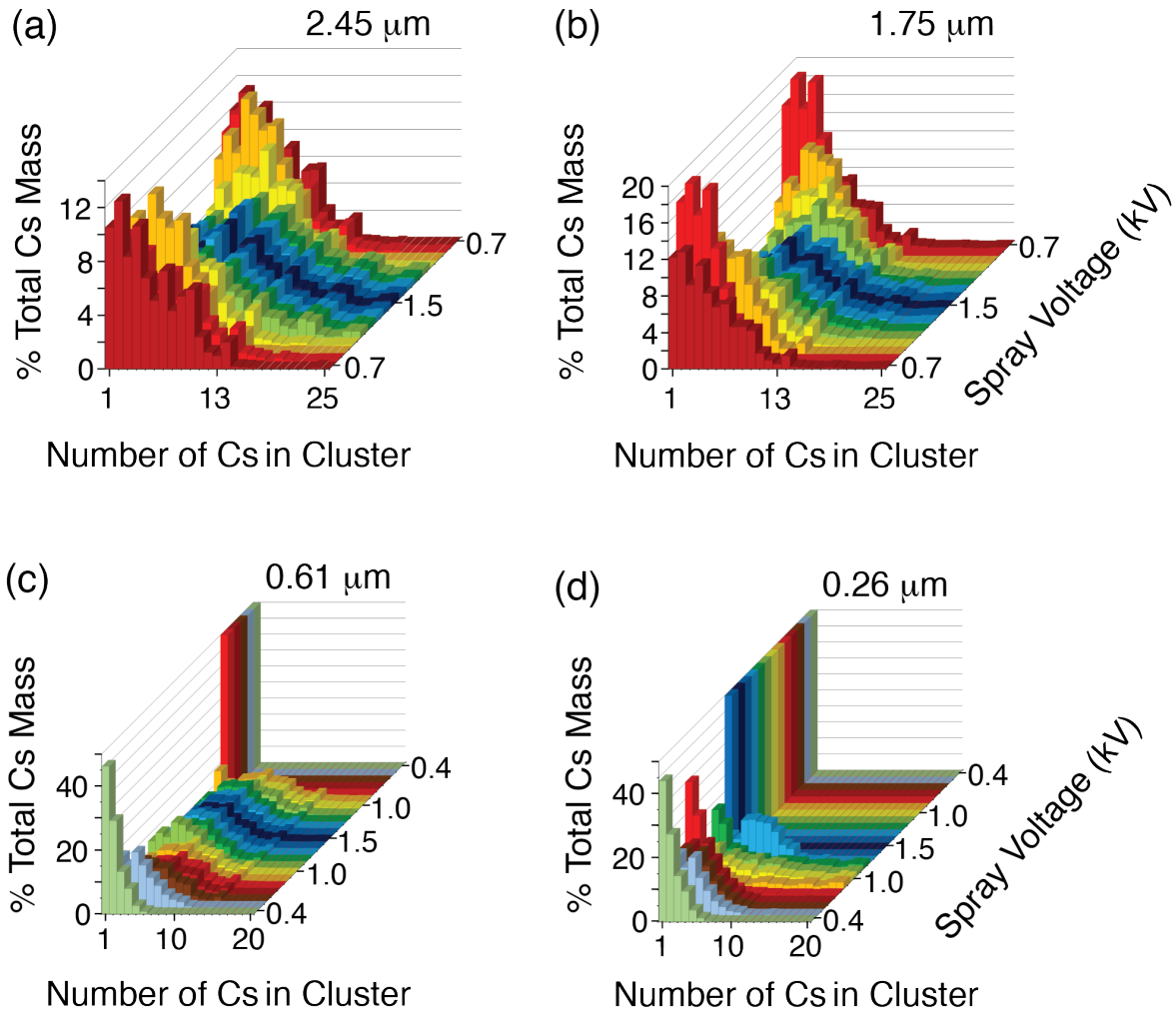

Figure 1. Representative cluster distributions obtained from 10 mM CsI as a function of electrospray voltage and emitter tip size of (a) ~2.45 μm, (b) ~1.75 μm, (c) 0.61 μm, and (d) 0.26 μm. Larger tips show cluster size distributions that change reproducibly with spray voltage, but the smallest tips in (c) and (d), undergo a transition that results in only formation of Cs^+ and $Cs(H_2O)^+$. The cluster distributions from submicron emitters have greater variability with increasing spray voltage that may be related to changes in the electrospray mode.

For 260 nm emitters, Cs^+ is 47.6 ± 3.7% and 15.3 ± 6.0% of the total Cs mass at 0.4 kV and 1.1 kV, respectively. The fractional mass of singly charged clusters increases from 52.0 ± 1.4% to 64.4 ± 3.2%, and the fraction of multiply (+2, +3) charged clusters increases from 0.4 ± 0.5% to 21.1 ± 15.2% across the same range of spray voltages. The higher uncertainty in the fraction of multiply charged clusters produced from 260 nm tips may be related to changes in the electrospray mode that occur when spraying from submicron emitters (Figure 1c,d).

CsI is highly soluble in water (848 g/L or ~3.3 M at 25 °C)[40] so extensive clustering or ion pairing in solution at the original solution concentrations is not expected. Both emitter tip size and voltage can affect the initial droplet size that is formed by electrospray with larger emitters and higher voltages leading to higher solution flow rates and larger initial droplet sizes.[7,8] Solvent evaporation can lead to nonspecific aggregation and cluster formation in the ESI droplet prior to gaseous ion formation resulting in formation of salt clusters.[7,10,41] The abundances and maximum size of these clusters can indicate the original size of an ESI droplet.[7] The population and size of clusters decreases with emitter tip size at 1.0 kV, consistent with smaller emitters producing smaller initial droplet sizes and hence less clustering (Figure 1a, 1b, 1c, 1d). At the lowest spray voltage for each emitter size and 100 μM concentrations, Cs^+ is >90% of the total Cs mass across all tip sizes compared to values of 8.4 ± 2.3%, 7.7 ± 5.1 %, 54.4 ± 5.2% and 47.6 ± 3.7% from 2.45 μm, 1.75 μm, 608 nm, and 260 nm at 10 mM concentrations, respectively (Figure S1). These data are consistent with fewer CsI ions within each initially formed electrospray droplet at lower solution concentrations, smaller emitter tip diameters, and at lower electrospray voltages. All of these factors reduce non-specific cluster formation or aggregation during ESI owing to the formation of smaller initial droplets.

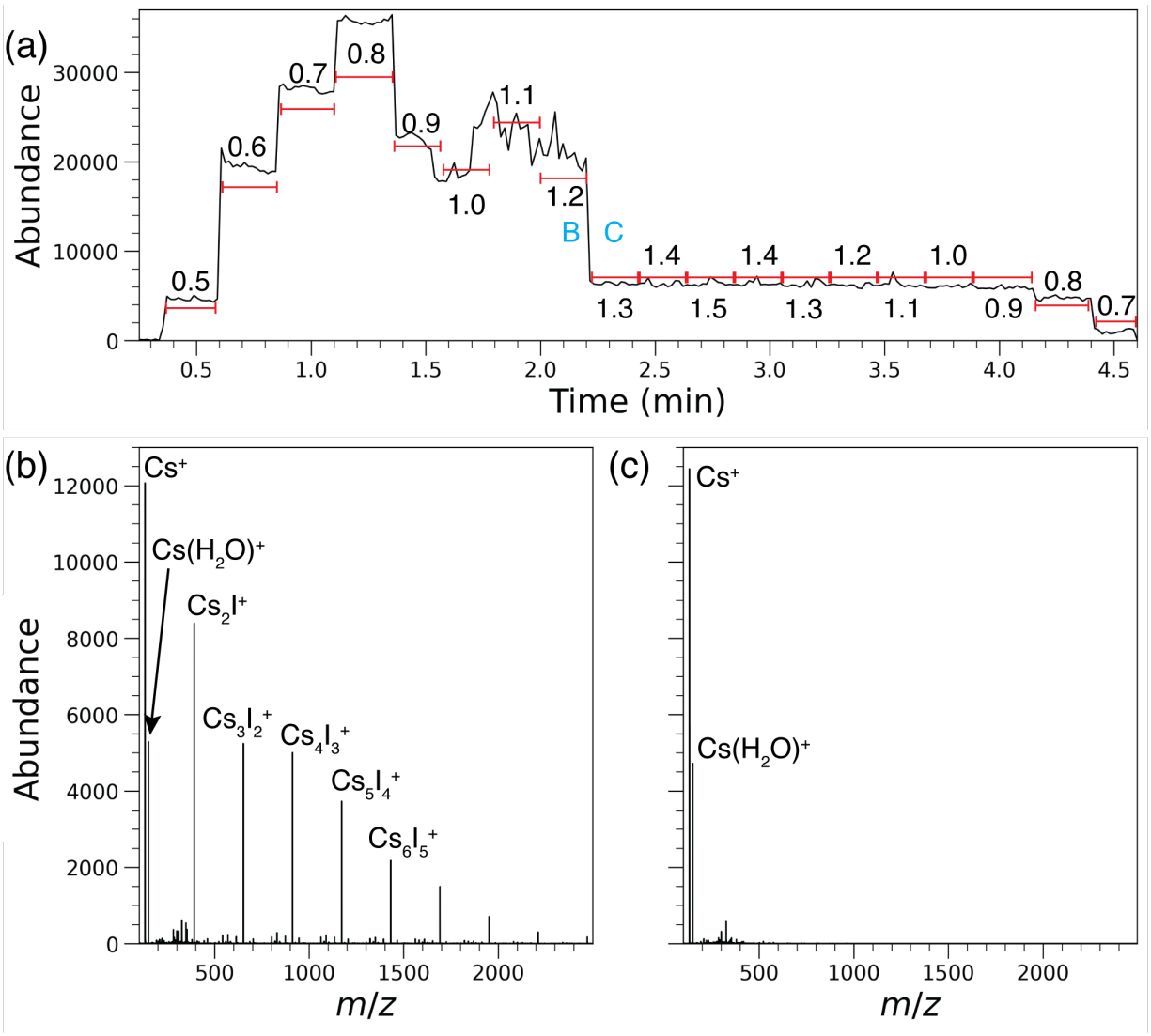

Figure 2. (a) Representative total ion current resulting from electrospray of a 10 mM CsI solution as a function of time from an emitter with ~608 nm diameter tip showing a significant reduction in total ion current that occurs upon corona discharge. The numbers above each time increment indicate the spray voltage in kV. Representative mass spectra from time periods labeled B and C are shown in (b) and (c), respectively. The abundance values on the *y*-axis are the same in (b) and (c), indicating that the abundance of Cs^+ is similar before and after corona discharge.

For emitters with tips larger than 1 μm, the change in cluster distributions with increasing voltage were the same as those observed when the voltage was decreased (Figures 1a, 1b). However, for emitters with diameters smaller than 1 μm, decreasing the voltage after reaching 1.5 kV results in the disappearance of CsI clusters from the mass spectra (Figures 1c, 1d). With the 608 nm emitters, increasing the spray voltage from 0.8 kV to 1.5 kV can lead to a large drop (typically ~50-80%) in the total ion signal (Figure 2a, between points labeled B and C). The time at which this drop in current occurs upon reaching voltages >0.8 kV is highly variable between emitters, with the fastest occurring immediately upon reaching 0.8 kV (~1.1 min from the start of spray) and the latest occurring upon a second ramp in voltage at 0.9 kV (~7 min from start of spray). This reduction in current occurred upon the first voltage ramp in 12 out of 15 replicates with different 608 nm emitters, typically at voltages of ~1.0 – 1.5 kV. In contrast, this drop in current occurred for every 260 nm emitter upon the first voltage ramp. Across all experiments using submicron diameter tips, the onset voltage for ion formation (0.4 kV) is not significantly different before and after this transition (Figure S2). The change in ion current between ~1.3 – 2.2 min (Figure 2a) is likely a result of a change in the spraying mode. Abundant CsI clusters are observed during this time period. When spraying 10 mM CsI from 608 nm diameter emitters at 1.2 kV, abundant CsI clusters were observed prior to this drop in current (Figure 2b). After this transition, there is abundant Cs^+ and some $Cs(H_2O)^+$ but no clusters of CsI (Figure 2c). Experiments were performed under gentle conditions to minimize gas-phase dissociation, as demonstrated by the abundant water adduct to Cs^+ at *m/z* ~151 (Figure 2b and 2c). Dissociation of this ion results in formation of Cs^+ confirming the identity of this ion.

In order to determine if the large drop in ion current initiated by higher voltages in the emitters with the small tips is accompanied by a change in the solution flow rate, the flow rate of

a 608 nm emitter was determined by measuring the change in the mass of the emitter over 5 min while spraying at 1.0 kV.[42–44] Solvent loss also occurs due to evaporation, the rate of which can be determined from changes in mass without an applied voltage. Solvent evaporation occurs at a rate of 2.0 ± 0.2 nL min^{-1}. The flow rates before and after the significant drop in total ion current with voltage applied after subtracting the water lost to evaporation were 5.0 ± 3.6 nL min^{-1} and 0.1 ± 0.3 nL min^{-1}, respectively. The higher uncertainty during standard spray is due to variations in flow from the different emitters and could be due to small differences in emitter position or morphology, which are not factors in evaporative loss. After the transition, the mass loss due to solution flow is indistinguishable from the evaporation rate, yet the abundance of the Cs^+ ion indicates that ion formation from the emitter still occurs.

Imaging submicron diameter emitters during electrospray

Emitter tips were visually monitored during electrospray using a Dino-Lite digital microscope camera (50x maximum magnification) and a 20x objective lens mounted to the mass spectrometer source housing. Ions were formed from a 10 mM aqueous CsI solution and emitters with a tip diameter of 608 nm at voltages between 0.8 and 1.5 kV. Below 1.0 kV, the emitter tips are clear (Figure 3a). The large drop in the total ion current corresponds to what appears to be the onset of corona discharge at the end of the emitter (Figure 3b, supporting video 1). Light emission is commonly observed at the onset of corona discharge initiated at high voltages.[45–47] Material is observed at the end of the emitter after discharge occurs (Figure 3c, supporting video 1). Scanning electron microscopy images of these emitters after drying overnight indicate that there is no observable change to the inner diameter of the emitters (Figure 3d). The resolution of the SEM at 10000x magnification is ~16.3 nm/pixel, indicating that any changes to the tip size

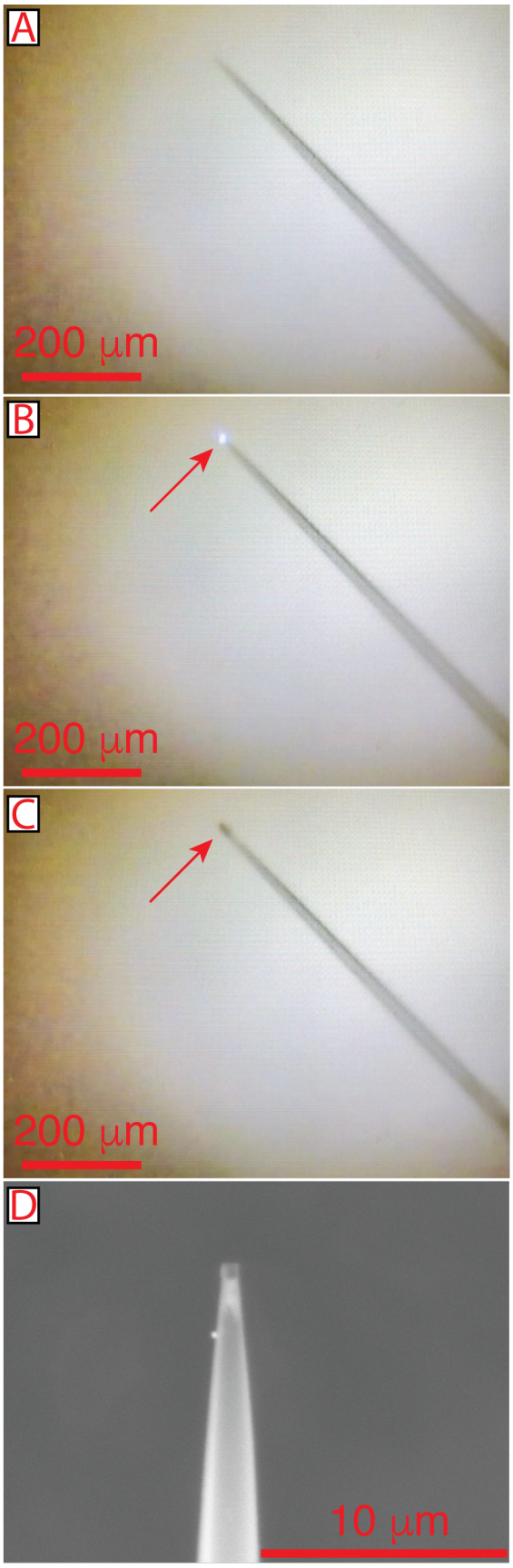
A
200 μm
B
200 μm
C
200 μm
D
10 μm

Figure 3. Optical and scanning electron microscope images of a single emitter with a 608 nm diameter tip used to spray a 10 mM CsI aqueous solution: (a) at low spray voltages (<1 kV), emitters appear to have transparent tips and mass spectra show a distribution of Cs_nI_{n-1} clusters (Figure 2b). At voltages between 1 and 1.5 kV, (b) corona discharge may occur, resulting in mass spectra where Cs^+ is the most abundant ion (Figure 2c). After corona discharge, (c) visible material is present at the tip of the emitter. (d) scanning electron microscopy image obtained from an emitter that was dried overnight reveals no change to the inner diameter or to the rest of the tip, indicating that corona discharge does not damage the borosilicate glass. Material can often be dislodged at higher voltages and a return to normal electrospray occurs further indicating that the emitters are not damaged by the discharge.

and shape that may have occurred are less than ~16 nm. The image shows material at the end of the capillary, consistent with what was observed optically after discharge. However, crystallized CsI after water evaporation may also contribute significantly to the deposited material in this image.

The SEM data indicate that the corona discharge process does not irreversibly damage the emitters, but that material build-up at the end of the emitter disrupts the spray process. This material appears after corona discharge even when a blank containing just pure milliQ water was used. Passing the milliQ water through a 0.22 μm filter did not affect the appearance of this material indicating that if any microorganisms or particles larger than this are present in the water, they do not contribute to this material buildup. Increasing the spray voltage by ~500 V can dislodge the material, restoring spray along with formation of clusters.

The abundant signal for Cs^+ post-discharge shows that ions are still generated from the ESI emitter despite a flow rate too low to measure. The disappearance of CsI clusters indicates that larger droplets capable of containing multiple Cs^+ and I^- are not being formed consistent with the unmeasureable flow rate. The discharge may partially block the aperture of the emitter with debris, resulting in the production of small droplets such that each droplet contains few ions preventing the formation of CsI clusters. Ions can also be produced by desorption from crystals. In field desorption mass spectrometry (FD-MS), ions are produced by applying a high voltage (8 – 20 kV) and heat (>100 °C) to crystalline samples deposited onto a filament. For inorganic salts, the most abundant ions tend to be the bare cation and clusters of the form $[C + (CA)_n]^+$, where C and A are the cation and anion, respectively.[48,49] Schulten and Rollgen observed clusters with up to six sodium acetate molecules are formed from sodium acetate crystals and Rollgen *et al.* reported $Ca_2Cl_2^{2+}$ in FD mass spectra of $CaCl_2$ crystals.[48,50] The absence of cluster ions after

corona discharge from submicron emitters suggests that the ions are not desorbed from a solid crystal.

A change to the emitter opening may also affect the electric field at the air-water interface, potentially resulting in the desorption of ions directly from the tip of the emitter. In this case, the abundance of ions after discharge are expected to follow trends in the solvation energy of the cations. To investigate this apparent desorption process after corona discharge, solutions containing Cs^+ and other cations of varying solvation energies were formed by electrospray and the abundance of these cations before and after discharge were compared.

Effects of Ion Solvation Energy

nESI mass spectra of an aqueous solution containing $BaCl_2$ and CsCl from an emitter with a 608 nm tip show abundant $Ba(H_2O)_{0\text{-}4}^{2+}$ in addition to clusters of the form $Cs_nCl_{n\text{-}1}^+$, $Ba_nCl_{2n\text{-}1}^+$, $Ba_nCl_{2n\text{-}2}^{2+}$ and mixed clusters containing both Ba^{2+} and Cs^+ (Figure 4a). After discharge is induced at a voltage of 1.5 kV, Cs^+ and $Cs(H_2O)^+$ are over 97% of the ion signal and no Ba^{2+} or Ba-containing cluster ions are detected (Figure 4b). Some minor peaks (<2.5% of the total ion abundance) are attributed to Cs-adducted background organic contaminants also present in the solvent blank, which may contribute to material build up at the end of the emitter. The abundances of Ba^{2+} and $Ba(H_2O)_{1\text{-}4}^{2+}$ relative to the abundances of Cs^+ and $Cs(H_2O)^+$ before and after discharge were determined. This value prior to discharge was 2.66 and after discharge was less than 1.46×10^{-4}. The value after discharge is an upper limit determined from the noise level in these spectra. The ratio of these values before and after discharge, abbreviated as the ratio of relative abundances (RRA), is <0.00035. The absence of detectable Ba^{2+} and $Ba(H_2O)_{1\text{-}4}^{2+}$ after discharge indicates that droplets are not formed, yet abundant Cs^+ signal shows that selective ion

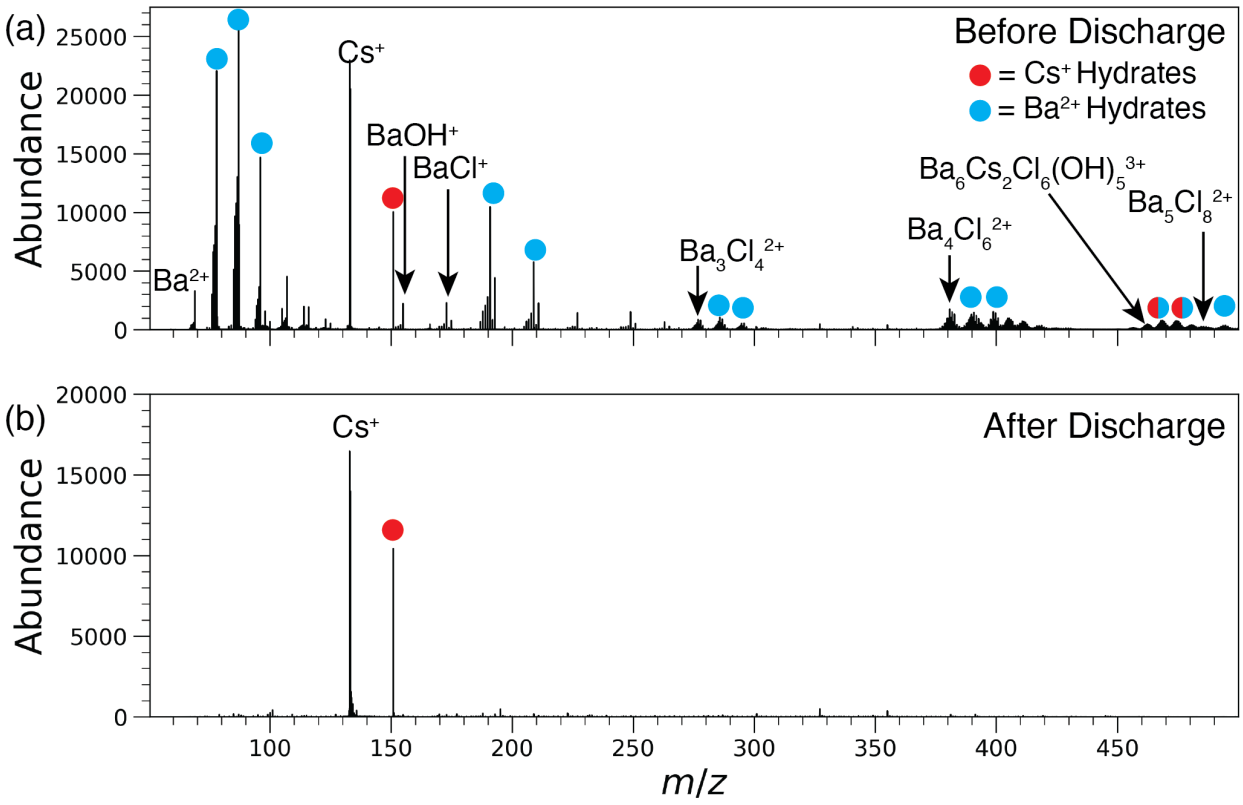

Figure 4. nESI mass spectra of an aqueous solution of 5 mM $BaCl_2$ and 5 mM CsCl obtained with an emitter with a 608 nm diameter tip (a) before and (b) after corona discharge.

formation still occurs. The Gibbs solvation free energy (GSFE) of Cs^+ is 800 kJ mol^{-1} compared to -200 kJ mol^{-1} for Ba^{2+} (all values are referenced to H^+),[51] indicating that the energetic cost to remove Ba^{2+} from water is substantially larger than for Cs^+. These data are consistent with desorption of Cs^+ directly from solution at the tip of the emitter whereas Ba^{2+} is retained in water due to its more negative GSFE value.

Tetraethylammonium, TEA^+, has a higher Gibbs solvation free energy (GSFE = 1050 kJ mol^{-1})[51] than Cs^+. A nESI spectrum of an equimolar aqueous solution of TEACl and CsCl obtained using emitters with 608 nm tip diameters results in TEA^+, Cs^+ and $Cs(H_2O)^+$ in nearly equal abundances (Figure S3a). Singly charged clusters with CsCl and TEACl are also observed. After discharge, TEA^+, Cs^+ and $Cs(H_2O)^+$ are the dominant ion signal (Figure S3b) and no clusters are observed. The RRA_{TEA} value of 0.77 indicates that TEA^+ relative to Cs^+ does not change significantly after discharge. There are many differences in the physical properties of Ba^{2+} compared to TEA^+, but the striking difference in RRA values for Ba^{2+} (<0.00035) compared to TEA^+ (0.77) suggests that this may be due to their large difference in GSFE values (~1250 kJ mol^{-1}).

The effects of Gibbs solvation free energy on RRA values for cations with intermediate GSFE values were investigated. Results for Rb^+, K^+, Na^+, Li^+, and Cu^{1+}, along with Cs^+, Ba^{2+}, and TEA^+ are shown in Figure 5. Results for ions with low *m*/*z* are more challenging to detect in the Q-TOF instrument due to poor transmission efficiency. To account for this, the instrument settings were tuned to favor lower *m*/*z* ions and favor the transmission of hydrated clusters that have higher *m*/*z* by increasing the sample cone voltage. The GSFE value for Rb^+ (GSFE = 775 kJ mol^{-1})[51] is similar to Cs^+ and Rb^+ has a RRA of ~1 (Figure 5, Figure S4). RRA values for K^+ (GSFE = 755 kJ mol^{-1}), Na^+ (GSFE = 685 kJ mol^{-1}) and Li^+ (GSFE = 575 kJ mol^{-1}) determined

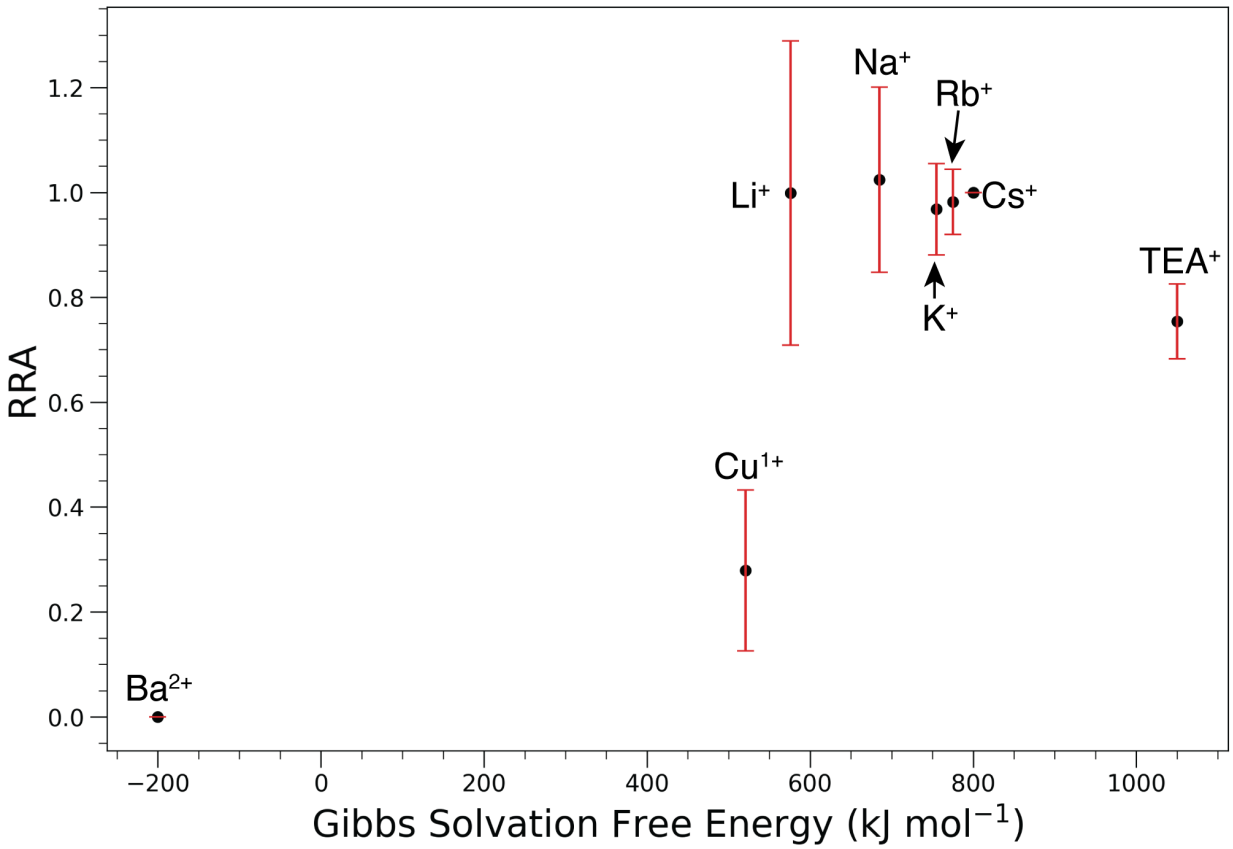

Figure 5. The ratio of relative abundances of cations to Cs^+ before and after the discharge event (RRA) as a function of Gibbs solvation free energy (GSFE). Error bars represent the standard deviation of the RRA value measured with three different emitters. Ions with GSFE values lower than ~540 kJ mol^{-1} are significantly suppressed or not observed after discharge.

from the abundances of $X(H_2O)_{0-4}^+$ (X = K, Na, Li) are 0.97, 1.03, and 1.00 respectively (Figures S5, S6, and S7, respectively).[51] The RRA for Cu^{1+} (GSFE = 521 kJ mol^{-1})[51] determined from the abundances of $Cu(H_2O)_{0-3}^{1+}$ is 0.28, suggesting that this ion is near the energetic threshold for desorption (Figure S8). A corona discharge reproducibly occurred at ~0.7 kV with the CuCl:CsCl solution. This may be related to the saturated concentration of CuCl that was used in these samples. The presence of undissolved solids or crystallization near the tip of the emitter could create an irregular surface more prone to corona discharge at lower voltages. Further increasing the spray voltage from 0.7 kV to 1.5 kV resulted in no significant change in the RRA. Ions corresponding to $Cu(H_2O)_{0-2}(OH)^+$ were also observed before and after discharge with an RRA of 0.21. No doubly charged copper or copper clusters (GSFE = -960 kJ mol^{-1})[51] were observed, consistent with results from Ba^{2+} that indicate doubly charged ions do not desorb from the emitter due to more negative solvation energies. These data suggest that $Cu(II)(OH)^+$ desorbs from the emitter as a singly charged ion and likely has a similar GSFE to Cu^+. Ions with GSFE values higher than ~540 kJ mol^{-1} (where the RRA = 0.5 between Cu^{1+} and Li^+) are formed both before and after discharge occurs whereas below this value, ions are significantly suppressed or eliminated after discharge occurs.

After discharge, the absence of cluster ions and ions that have GSFE values below ~540 kJ mol^{-1} indicates that droplets are no longer being formed. If droplet formation still occurred after discharge, then ions with low GSFE values should still incorporate into the droplets and result in ion formation. The absence of these ions and cluster ions indicates that ions with GSFE values above ~540 kJ mol^{-1} are formed by desorption directly from the emitter after discharge. To desorb, ions must overcome an energy barrier due to the GSFE. Energy related to any surface deformation that may be necessary to emit ions also contributes to this energetic barrier. High

electric fields at the air-water interface, which depend on interface size and applied voltage, may drive this process. After corona discharge, the appearance of material at the end of the emitter could reduce the effective diameter of the emitter or may lead to uneven surface morphology that may promote distortion of water at the interface. In both cases, the result is a much larger effective electric field at the air-water interface, which may drive desorption directly from the solution contained within the emitter without the formation of nanodroplets. Thomson and Iribarne[52] noted that multiply charged cations showed no evidence of evaporation, consistent with the more negative solvation energies of these analytes.[51]

Cooks and coworkers have suggested that the strong electric fields and irregular morphology at the tip of paper emitters could cause ions to desorb from solution during paper spray ionization.[53,54] It is possible that a similar mechanism occurs for submicron emitters due to material build-up at the emitter tip after corona discharge, which may form an irregular surface with strong electric fields at the tip that allows ions to desorb directly from solution.

Desorption of peptides and proteins from a charged air-liquid interface

In order to investigate whether desorption of peptides and proteins can also occur directly from charged air-water interfaces, mass spectra of aqueous solutions of 5 mM $BaCl_2$, 5 mM CsCl and 10 μM bradykinin or ubiquitin were acquired using emitters with 608 nm diameter tips both pre- and post-corona discharge. The presence or absence of Ba^{2+} in the mass spectra along with the presence or absence of $Cs(CsCl)_n^+$ was used to indicate whether droplets were formed after discharge. For solutions with bradykinin, both Ba^{2+} and $Cs(CsCl)_n^+$ are observed at voltages below 1 kV indicating that ion formation from droplets occurs. Protonated, Cs-adducted, and Ba-adducted bradykinin ions with charge states between +1 and +3 are also observed (Figure 6a).

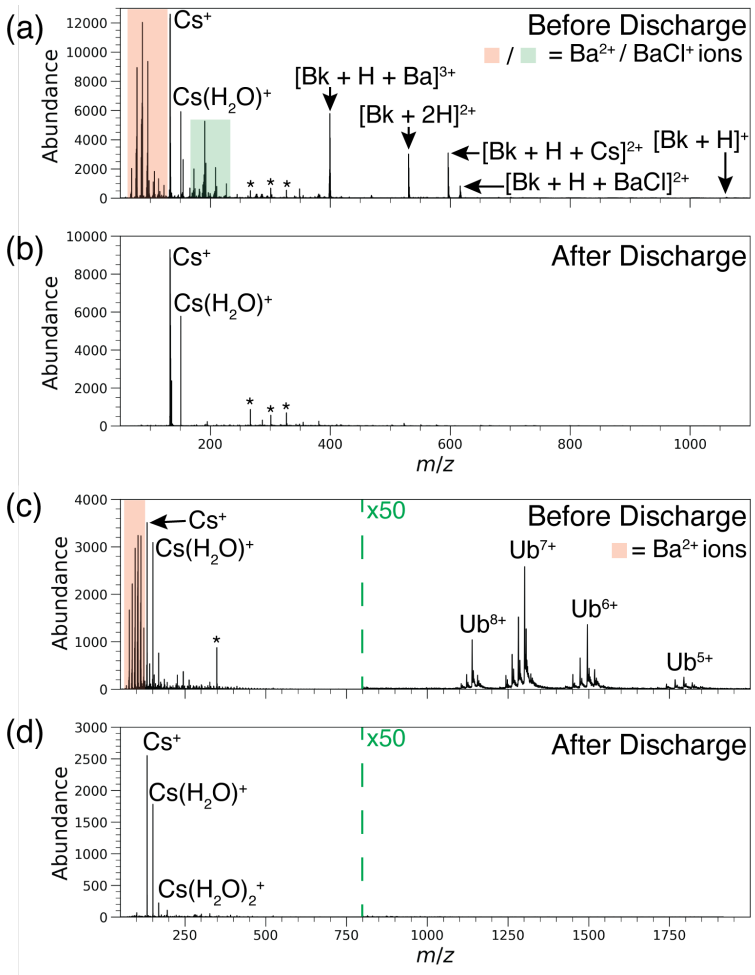

Figure 6. nESI mass spectra of a 10 µm solution of bradykinin (a,b) or ubiquitin (c,d) in 1:1 CsCl:$BaCl_2$ obtained from an emitter with a 608 nm diameter tip before and after corona discharge. Light red and green regions indicate Ba^{2+} and $BaCl^+$ ions, respectively, and associated hydrates. Prior to discharge, bradykinin and ubiquitin ions are observed with cesium and barium adduction, consistent with formation of these ions from nanodrops. After discharge, abundant Cs^+ is observed, but bradykinin, ubiquitin or barium ions are not, consistent with desorption of Cs^+, but not Ba^{2+}, bradykinin, or ubiquitin. Asterisk indicates Cs-adducted organic contaminants that were confirmed by MS/MS. Regions from 800 – 2000 *m/z* are expanded by 50x in (c) and (d).

Cs- and Ba-adduction to bradykinin only occurs for the +2 and +3 charge states. Increasing the spray voltage to ~1.3 kV induced corona-discharge. After discharge, there are no bradykinin ions of any form, nor are Ba^{2+} or $Cs(CsCl)_n^+$ formed. However, abundant Cs^+ and $Cs(H_2O)_1^+$ are observed indicating selective ion formation continues after the discharge (Figure 6b). After discharge, several ions corresponding to Cs-adducted organic contaminant ions are also observed at low abundance (<10% relative to Cs^+) as confirmed by MS/MS experiments. These results indicate that under conditions where Cs^+ appears to readily desorb from the emitter tip after discharge, bradykinin ions do not. Prior measurements during sustained corona discharge for large metal electrospray emitters indicate that there can be more consistent peptide signal during the discharge, but the spectra are otherwise unaffected.[45]

Similar results were obtained from these same experiments where ubiquitin was added in place of bradykinin. Prior to discharge, ubiquitin ions with charge states between +5 and +8 and extensive Cs-adduction are observed (Figure 6c). After discharge, there are no ubiquitin ions, Ba^{2+} or $Cs(CsCl)_n^+$ but abundant Cs^+ and $Cs(H_2O)_{1,2}^+$ remain (Figure 6d). The absence of protein ion signal after discharge indicates that ubiquitin does not desorb from solution at the tip of the emitter under the voltages and tip diameters employed here (Figure 6c,d). It has been speculated that proteins can desorb directly from the air-water interface from much larger emitters at higher spray voltages.[55] Li *et al.* reported the disappearance of cytochrome *c* signal during femtoelectrospray of a mixture of cytochrome *c* and the peptide MRFA from 30 – 160 nm emitters at spray voltages between 0.4 – 2.0 kV.[9] Interestingly, solvent evaporation was not blocked and MRFA signal was still observed after the loss of protein signal. This effect was attributed to size-selective partial clogging of the emitter that preferentially filtered out larger protein molecules. The ionic diameters of Cu^{1+}, Ba^{2+}, Cs^+, TEA^+, bradykinin, and ubiquitin are

~0.09 nm (coordination II),[56] ~0.27 nm (coordination VI),[56] ~0.33 nm (coordination VI),[56] ~0.77 nm,[57] ~1.14 nm (approximated from calculated topological surface area and assuming a sphere), and ~2.64 nm (native form, calculated from radius of gyration),[58] respectively. Ba^{2+} and Cu^{1+} are among the smallest ions, yet they have the lowest RRA values. The hydrated diameter of ions can be significantly larger than the ionic diameter. The hydrated diameter of Ba^{2+} (0.81 nm)[59], is nearly the same as that of TEA^{+} (0.80 nm),[59] yet these two ions have significantly different RRA values of ~0 and ~0.77, respectively. These data indicate that size-selective partial clogging of the emitters is not the cause for the absence of Ba^{2+} or peptide and protein signal in our experiments. The high solubility limit of ubiquitin and bradykinin (>1 mM) suggests that these molecules have significant negative solvation energies, consistent with desorption being an unfavorable process for their transfer into the gas-phase.

Conclusion

The electrospray voltage and emitter tip diameter have a significant effect on the size distribution of CsI clusters indicating a significant effect on the size of the initial droplets that are formed. The least clustering occurs at the lowest voltage where stable spray is obtained at any tip size and clustering increases with larger diameter tips and higher solution concentrations. Changing the voltage on emitters with tip diameters greater than ~1 μm leads to a reproducible change in cluster size independent of raising or lowering the voltage between 0.4 kV and 1.5 kV. In contrast, corona discharge reproducibly occurred for emitters with 260 nm diameter tips at voltages >1.2 kV. Material deposition at the emitter tip occurs and leads to a flow rate that is too low to measure despite continued formation of Cs^{+} but no CsI clusters. Under these conditions, ions such as Ba^{2+} are not observed nor are ions of bradykinin or ubiquitin which are readily

ionized pre-discharge. These results indicate that ions with more positive solvation energies can be desorbed directly from the solution-air interface whereas those with negative and less positive (<540 kJ mol^{-1}) solvation energies are not.

Results from some molecular dynamics simulations indicate that peptides and proteins can be desorbed from charged droplets either as an extended chain or as intact, folded complexes.[60–62] Our results indicate that under conditions where ion desorption from the liquid-air interface occurs for Cs^+, Rb^+, K^+, Na^+, Li^+ and Cu^+, desorption of peptides and proteins does not occur consistent with a large negative solvation energy for these ions. Future work with emitters with even smaller tip diameters may shed additional light into ion formation mechanisms in electrospray ionization.

Supporting Information

Video showing corona discharge and material buildup at the end of a 608 nm emitter; Cluster distributions from 100 μM CsI as a function of spray voltage; Representative TIC collected from 10 mM CsI from a 608 nm emitter; Mass spectra of XCl:CsCl (X = TEA, Rb, K, Na, Li, Cu) solutions before and after corona discharge was observed. Table containing *m/z* and charge of recurring organic contaminant ions.

Acknowledgments

The authors thank Dr. Anthony T. Iavarone for help with instrumentation and insightful discussions, as well as the staff at the University of California, Berkeley Electron Microscopy Laboratory for advice on electrospray emitter imaging. This material is based on work supported by the National Science Foundation Division of Chemistry under grant number CHE-2203907, a

NSF Graduate Research Fellowship for JSJ (DGE-2146752), and the Merck DBL SEEDS program.

References

(1) Marginean, I.; Kelly, R. T.; Prior, D. C.; LaMarche, B. L.; Tang, K.; Smith, R. D. Analytical Characterization of the Electrospray Ion Source in the Nanoflow Regime. *Anal. Chem.* **2008**, *80*, 6573–6579.

(2) Wilm, M.; Mann, M. Analytical Properties of the Nanoelectrospray Ion Source. *Anal. Chem.* **1996**, *68*, 1–8.

(3) Susa, A. C.; Xia, Z.; Williams, E. R. Native Mass Spectrometry from Common Buffers with Salts That Mimic the Extracellular Environment. *Angew. Chem. Int. Ed.* **2017**, *56*, 7912–7915.

(4) Susa, A. C.; Xia, Z.; Williams, E. R. Small Emitter Tips for Native Mass Spectrometry of Proteins and Protein Complexes from Nonvolatile Buffers That Mimic the Intracellular Environment. *Anal. Chem.* **2017**, *89*, 3116–3122.

(5) Susa, A. C.; Lippens, J. L.; Xia, Z.; Loo, J. A.; Campuzano, I. D. G.; Williams, E. R. Submicrometer Emitter ESI Tips for Native Mass Spectrometry of Membrane Proteins in Ionic and Nonionic Detergents. *J. Am. Soc. Mass Spectrom.* **2018**, *29*, 203–206.

(6) Yuill, E. M.; Sa, N.; Ray, S. J.; Hieftje, G. M.; Baker, L. A. Electrospray Ionization from Nanopipette Emitters with Tip Diameters of Less than 100 nm. *Anal. Chem.* **2013**, *85*, 8498–8502.

(7) Davidson, K. L.; Oberreit, D. R.; Hogan, C. J.; Bush, M. F. Nonspecific Aggregation in Native Electrokinetic Nanoelectrospray Ionization. *Int. J. Mass Spectrom.* **2017**, *420*, 35–42.

(8) Hollerbach, A.; Logsdon, D.; Iyer, K.; Li, A.; Schaber, J. A.; Graham Cooks, R. Sizing Sub-Diffraction Limit Electrosprayed Droplets by Structured Illumination Microscopy. *Analyst* **2018**, *143*, 232–240.

(9) Li, H.; Allen, N.; Li, M.; Li, A. Conducting and Characterizing Femto Flow Electrospray Ionization. *Analyst* **2022**, *147*, 1071–1075.

(10) Jordan, J. S.; Williams, E. R. Effects of Electrospray Droplet Size on Analyte Aggregation: Evidence for Serine Octamer in Solution. *Anal. Chem.* **2021**, *93*, 1725–1731.

(11) Jordan, J. S.; Williams, E. R. Homochiral Preference of Serine Octamer in Solution and Formed by Dissociation of Large Gaseous Clusters. *Analyst* **2021**, *146*, 6822–6830.

(12) Nguyen, G. T. H.; Nocentini, A.; Angeli, A.; Gratteri, P.; Supuran, C. T.; Donald, W. A. Perfluoroalkyl Substances of Significant Environmental Concern Can Strongly Inhibit Human Carbonic Anhydrase Isozymes. *Anal. Chem.* **2020**, *92*, 4614–4622.

(13) Nguyen, G. T. H.; Tran, T. N.; Podgorski, M. N.; Bell, S. G.; Supuran, C. T.; Donald, W. A. Nanoscale Ion Emitters in Native Mass Spectrometry for Measuring Ligand–Protein Binding Affinities. *ACS Cent. Sci.* **2019**, *5*, 308–318.

(14) Nguyen, G. T. H.; Bennett, J. L.; Liu, S.; Hancock, S. E.; Winter, D. L.; Glover, D. J.; Donald, W. A. Multiplexed Screening of Thousands of Natural Products for Protein–

Ligand Binding in Native Mass Spectrometry. *J. Am. Chem. Soc.* **2021**, *143*, 21379–21387.
(15) Báez Bolivar, E. G.; Bui, D. T.; Kitova, E. N.; Han, L.; Zheng, R. B.; Luber, E. J.; Sayed, S. Y.; Mahal, L. K.; Klassen, J. S. Submicron Emitters Enable Reliable Quantification of Weak Protein-Glycan Interactions by ESI-MS. *Anal. Chem.* **2021**, *93*, 4231–4239.
(16) Agasid, M. T.; Sørensen, L.; Urner, L. H.; Yan, J.; Robinson, C. V. The Effects of Sodium Ions on Ligand Binding and Conformational States of G Protein-Coupled Receptors-Insights from Mass Spectrometry. *J. Am. Chem. Soc.* **2021**, *143*, 4085–4089.
(17) Bui, D. T.; Li, Z.; Kitov, P. I.; Han, L.; Kitova, E. N.; Fortier, M.; Fuselier, C.; Granger Joly de Boissel, P.; Chatenet, D.; Doucet, N.; Tompkins, S. M.; St-Pierre, Y.; Mahal, L. K.; Klassen, J. S. Quantifying Biomolecular Interactions Using Slow Mixing Mode (SLOMO) Nanoflow ESI-MS. *ACS Cent. Sci.* **2022**, *8*, 963–974.
(18) Bennett, J. L.; Nguyen, G. T. H.; Donald, W. A. Protein–Small Molecule Interactions in Native Mass Spectrometry. *Chem. Rev.* **2022**, *122*, 7327–7385.
(19) Nguyen, G. T. H.; Leung, W. Y.; Tran, T. N.; Wang, H.; Murray, V.; Donald, W. A. Mechanism for the Binding of Netropsin to Hairpin DNA Revealed Using Nanoscale Ion Emitters in Native Mass Spectrometry. *Anal. Chem.* **2020**, *92*, 1130–1137.
(20) Lei, W.; Hu, J.; Chen, H.-Y.; Xu, J.-J. Combined Strategies for Suppressing Nonspecific Cationic Adduction to G-Quadruplexes in Electrospray Ionization Mass Spectrometry. *Anal. Chim. Acta.* **2022**, *1220*, 340146.
(21) Xia, Z.; Williams, E. R. Effect of Droplet Lifetime on Where Ions Are Formed in Electrospray Ionization. *Analyst* **2019**, *144*, 237–248.
(22) Smith, J. N.; Flagan, R. C.; Beauchamp, J. L. Droplet Evaporation and Discharge Dynamics in Electrospray Ionization. *J. Phys. Chem. A* **2002**, *106*, 9957–9967.
(23) Olumee, Z.; Callahan, J. H.; Vertes, A. Droplet Dynamics Changes in Electrostatic Sprays of Methanol−Water Mixtures. *J. Phys. Chem. A* **1998**, *102*, 9154–9160.
(24) Kim, J. Y.; Lee, S. J.; Baik, G. Y.; Hong, J. G. Viscosity Effect on the Electrospray Characteristics of Droplet Size and Distribution. *ACS Omega* **2021**, *6*, 29724–29734.
(25) Ku, B. K.; Kim, S. S. Electrospray Characteristics of Highly Viscous Liquids. *J. Aerosol Sci.* **2002**, *33*, 1361–1378.
(26) Gañán-Calvo, A. M.; Dávila, J.; Barrero, A. Current and Droplet Size in the Electrospraying of Liquids. Scaling Laws. *J. Aerosol Sci.* **1997**, *28*, 249–275.
(27) Tang, K.; Gomez, A. Monodisperse Electrosprays of Low Electric Conductivity Liquids in the Cone-Jet Mode. *J. Colloid Interface Sci.* **1996**, *184*, 500–511.
(28) Banerjee, S.; Mazumdar, S. Electrospray Ionization Mass Spectrometry: A Technique to Access the Information beyond the Molecular Weight of the Analyte. *Int. J. Anal. Chem.* **2012**, *2012*, 282574.
(29) Liyanage, O. T.; Brantley, M. R.; Calixte, E. I.; Solouki, T.; Shuford, K. L.; Gallagher, E. S. Characterization of Electrospray Ionization (ESI) Parameters on In-ESI Hydrogen/Deuterium Exchange of Carbohydrate-Metal Ion Adducts. *J. Am. Soc. Mass Spectrom.* **2019**, *30*, 235–247.
(30) Gomez, A.; Tang, K. Charge and Fission of Droplets in Electrostatic Sprays. *Phys. Fluids* **1994**, *6*, 404–414.
(31) Tang, K.; Gomez, A. Generation of Monodisperse Water Droplets from Electrosprays in a Corona-Assisted Cone-Jet Mode. *J. Colloid Interface Sci.* **1995**, *175*, 326–332.

(32) Juraschek, R.; Röllgen, F. W. Pulsation Phenomena during Electrospray Ionization. *Int. J. Mass Spectrom.* **1998**, *177*, 1–15.
(33) De La Mora, J. F.; Loscertales, I. G. The Current Emitted by Highly Conducting Taylor Cones. *J. Fluid Mech.* **1994**, *260*, 155–184.
(34) Pfeifer, R. J.; Hendricks, C. D. Parametric Studies of Electrohydrodynamic Spraying. *AIAA J.* **1968**, *6*, 496–502.
(35) Wilm, M. S.; Mann, M. Electrospray and Taylor-Cone Theory, Dole's Beam of Macromolecules at Last? *Int. J. Mass Spectrom. Ion Process* **1994**, *136*, 167–180.
(36) Schmidt, A.; Karas, M.; Dülcks, T. Effect of Different Solution Flow Rates on Analyte Ion Signals in Nano-ESI MS, or: When Does ESI Turn into Nano-ESI? *J. Am. Soc. Mass Spectrom.* **2003**, *14*, 492–500.
(37) Alexander, M. S.; Paine, M. D.; Stark, J. P. W. Pulsation Modes and the Effect of Applied Voltage on Current and Flow Rate in Nanoelectrospray. *Anal. Chem.* **2006**, *78*, 2658–2664.
(38) Jordan, J. S.; Xia, Z.; Williams, E. R. Tips on Making Tiny Tips: Secrets to Submicron Nanoelectrospray Emitters. *J. Am. Soc. Mass Spectrom.* **2022**, *33*, 607–611.
(39) Mortensen, D. N.; Williams, E. R. Theta-Glass Capillaries in Electrospray Ionization: Rapid Mixing and Short Droplet Lifetimes. *Anal. Chem.* **2014**, *86*, 9315–9321.
(40) Haynes, W. M. *CRC Handbook of Chemistry and Physics*; CRC Press, 2014.
(41) Gamero-Castaño, M.; Fernández De La Mora, J. Mechanisms of Electrospray Ionization of Singly and Multiply Charged Salt Clusters. *Anal. Chim. Acta* **2000**, *406*, 67–91.
(42) Mortensen, D. N.; Williams, E. R. Ultrafast (1 μs) Mixing and Fast Protein Folding in Nanodrops Monitored by Mass Spectrometry. *J. Am. Chem. Soc.* **2016**, *138*, 3453–3460.
(43) Mortensen, D. N.; Williams, E. R. Investigating Protein Folding and Unfolding in Electrospray Nanodrops Upon Rapid Mixing Using Theta-Glass Emitters. *Anal. Chem.* **2015**, *87*, 1281–1287.
(44) Mortensen, D. N.; Williams, E. R. Microsecond and Nanosecond Polyproline II Helix Formation in Aqueous Nanodrops Measured by Mass Spectrometry. *Chem. Commun.* **2016**, *52*, 12218–12221.
(45) Davis, E. J.; Walker, D.; Gibney, M.; Clowers, B. H. Optical and Mass Spectral Characterization of the Electrospray Ionization/Corona Discharge Ionization Interface. *Talanta* **2021**, *224*, 121870.
(46) Li, C.; Attanayake, K.; Valentine, S. J.; Li, P. Facile Improvement of Negative Ion Mode Electrospray Ionization Using Capillary Vibrating Sharp-Edge Spray Ionization. *Anal. Chem.* **2020**, *92*, 2492–2502.
(47) McClory, P. J.; Håkansson, K. Corona Discharge Suppression in Negative Ion Mode Nanoelectrospray Ionization via Trifluoroethanol Addition. *Anal. Chem.* **2017**, *89*, 10188–10193.
(48) Schulten, H. R.; Röllgen, F. W. On Field Desorption Mass Spectrometry of Salts. *Organic Mass Spectrometry* **1975**, *10*, 649–659.
(49) Lehmann, W. D.; Schulten, H. R. Determination of Alkali Elements by Field Desorption Mass Spectrometry. *Anal. Chem.* **1977**, *49*, 1744–1746.
(50) Röllgen, F. W.; Ott, K. H. On the Formation of Cluster Ions and Molecular Ions in Field Desorption of Salts. *Int. J. Mass Spectrom. Ion Physics* **1980**, *32*, 363–367.
(51) Marcus, Y. Thermodynamics of Solvation of Ions. Part 5.—Gibbs Free Energy of Hydration at 298.15 K. *J. Chem. Soc. Faraday Trans.* **1991**, *87*, 2995–2999.

(52) Thomson, B. A.; Iribarne, J. V. Field Induced Ion Evaporation from Liquid Surfaces at Atmospheric Pressure. *J. Chem. Phys.* **1979**, *71*, 4451–4463.
(53) Espy, R. D.; Muliadi, A. R.; Ouyang, Z.; Cooks, R. G. Spray Mechanism in Paper Spray Ionization. *Int. J. Mass Spectrom.* **2012**, *325–327*, 167–171.
(54) Li, A.; Wang, H.; Ouyang, Z.; Cooks, R. G. Paper Spray Ionization of Polar Analytes Using Non-Polar Solvents. *Chem. Commun.* **2011**, *47*, 2811.
(55) Siu, K. W. M.; Guevremont, R.; Le Blanc, J. C. Y.; O'Brien, R. T.; Berman, S. S. Is Droplet Evaporation Crucial in the Mechanism of Electrospray Mass Spectrometry? *Organic Mass Spectrometry* **1993**, *28*, 579–584.
(56) Shannon, R. D. Revised Effective Ionic Radii and Systematic Studies of Interatomic Distances in Halides and Chalcogenides. *Acta Crystallogr.* **1976**, *A32*, 751–767.
(57) Aue, D. H.; Webb, H. M.; Bowers, M. T. A Thermodynamic Analysis of Solvation Effects on the Basicities of Alkylamines. An Electrostatic Analysis of Substituent Effects. *J. Am. Chem. Soc.* **1976**, *98*, 318–329.
(58) Kamatari, Y. O.; Ohji, S.; Konno, T.; Seki, Y.; Soda, K.; Kataoka, M.; Akasaka, K. The Compact and Expanded Denatured Conformations of Apomyoglobin in the Methanol-Water Solvent. *Protein Sci.* **1999**, *8*, 873–882.
(59) Nightingale, E. R. Phenomenological Theory of Ion Solvation. Effective Radii of Hydrated Ions. *J. Phys. Chem.* **1959**, *63*, 1381–1387.
(60) Aliyari, E.; Konermann, L. Atomistic Insights into the Formation of Nonspecific Protein Complexes during Electrospray Ionization. *Anal. Chem.* **2021**, *93*, 12748–12757.
(61) Aliyari, E.; Konermann, L. Formation of Gaseous Proteins via the Ion Evaporation Model (IEM) in Electrospray Mass Spectrometry. *Anal. Chem.* **2020**, *92*, 10807–10814.
(62) Aliyari, E.; Konermann, L. Formation of Gaseous Peptide Ions from Electrospray Droplets: Competition between the Ion Evaporation Mechanism and Charged Residue Mechanism. *Anal. Chem.* **2022**, *94*, 7713–7721.

TOC Graphic

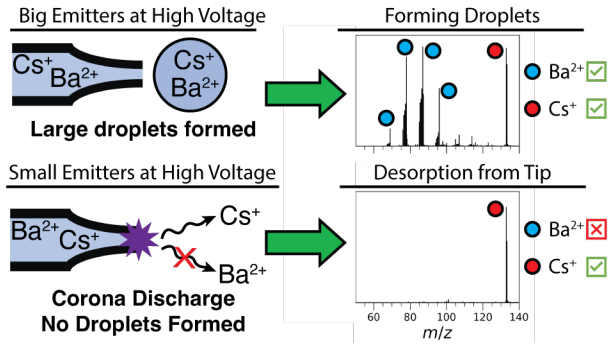
Big Emitters at High Voltage
Cs+ Ba2+
Cs+ Ba2+
Large droplets formed
Forming Droplets
Ba2+
Cs+
Small Emitters at High Voltage
Ba2+ Cs+
Cs+
Ba2+
Corona Discharge
No Droplets Formed
Desorption from Tip
Ba2+
Cs+
60 80 100 120 140
m/z